Environ. Sci. Technol. **2005**, *39,* 3679−3687

Spatial Variation in Deposition Rate Coefficients of an Adhesion-Deficient Bacterial Strain in Quartz Sand

MEIPING TONG,[†] TERRI A. CAMESANO,[‡] AND WILLIAM P. JOHNSON*,[†]

Department of Geology & Geophysics, University of Utah, Salt Lake City, Utah, and Department of Chemical Engineering, Worcester Polytechnic Institute, Worcester, Massachusetts

The transport of bacterial strain DA001 was examined in packed quartz sand under a variety of environmentally relevant ionic strength and flow conditions. Under all conditions, the retained bacterial concentrations decreased with distance from the column inlet at a rate that was faster than log-linear, indicating that the deposition rate coefficient decreased with increasing transport distance. The hyperexponential retained profile contrasted against the nonmonotonic retained profiles that had been previously observed for this same bacterial strain in glass bead porous media, demonstrating that the form of deviation from log-linear behavior is highly sensitive to system conditions. The deposition rate constants in quartz sand were orders of magnitude below those expected from filtration theory, even in the absence of electrostatic energy barriers. The degree of hyperexponential deviation of the retained profiles from log-linear behavior did not decrease with increasing ionic strength in quartz sand. These observations demonstrate that the observed low adhesion and deviation from log-linear behavior was not driven by electrostatic repulsion. Measurements of the interaction forces between DA001 cells and the silicon nitride tip of an atomic force microscope (AFM) showed that the bacterium possesses surface polymers with an average equilibrium length of 59.8 nm. AFM adhesion force measurements revealed low adhesion affinities between silicon nitride and DA001 polymers with ∼95% of adhesion forces having magnitudes <0.8 nN. Steric repulsion due to surface polymers was apparently responsible for the low adhesion to silicon nitride, indicating that steric interactions from extracellular polymers controlled DA001 adhesion deficiency and deviation from log-linear behavior on quartz sand.

Introduction

Investigations of colloid transport in porous media have recently focused on the profiles of retained colloids on porous media following transport experiments. This focus has yielded new insights such as the prevalence of deviation from expectations based on a spatially invariant deposition rate coefficient, which is expected to yield log decreases in retained concentrations with transport distance.

Deviations from log-linear decreases were first recognized in the bacterial transport literature (*1*) and have been corroborated by numerous subsequent transport studies of other biological colloids (*2*−*11*). Retained concentrations of microbes were observed to decrease faster than log-linear (hyperexponential decreases), indicating that the deposition rate coefficient decreased with distance of transport. These hyperexponential decreases in retained concentrations with distance of transport were tentatively attributed to distributions in the surface properties among the biological colloid population such that individual microbes more prone to retention were deposited near the column inlet and those less prone to retention were deposited further from the column inlet, if they deposited at all (*1*−*4*, *10*).

More recently, this same behavior was found to be characteristic of nonbiological colloids (carboxylate-modified polystyrene latex microspheres) (*12*, *13*). It should be noted that hyperexponential decreases in retained colloid concentrations have also been demonstrated to result from straining in some cases (*14*). However, the demonstrated sensitivity of the retained profiles to ionic strength precludes purely physical straining as the major process producing the observed deviations in many systems. Nonmonotonic deviation from log-linear retained profiles has also recently been described for bacteria (*15*) and for carboxylate-modified polystyrene latex microspheres (*16*), indicating that the form of deviation from log-linear behavior is not necessarily hyperexponential.

For the carboxylate-modified polystyrene latex microspheres, both hyperexponential and nonmonotonic deviation of the retained profile from log-linearity decreased with decreasing magnitude of the energy barrier to attachment (increased ionic strength). Deviation from log-linear retained profiles was eliminated under favorable conditions for the microspheres (*12*, *16*). The purpose of this paper is to demonstrate that the form of deviation from log-linear profiles of retained bacteria (strain DA001) is sensitive to system conditions. Furthermore, we demonstrate that adhesion deficiency of DA001 is driven by steric interactions from cell surface polymers, resulting in deviation from log-linear behavior that did not decrease with decreases in the energy barrier to deposition (increasing ionic strength).

Experimental Methods

Bacteria. Bacterial strain *Comamonas* DA001 was used in the experiments. DA001 is an adhesion-deficient, Gram-negative, nonmotile strain isolated from the shallow subsurface near Oyster, VA. The cells were approximately 1.1 μm by 0.3 μm in size with a density of roughly 1.06 g cm^{-3} (*17*).

Cells were grown at room temperature (22 °C) overnight while shaking at 120 rpm in filter-sterilized basal salts medium (BSM) supplemented with filter-sterilized 0.012 M sodium lactate. BSM consisted of 4.25 g of $K_2HPO_4 \cdot 3H_2O$, 1 g of $NaH_2PO_4 \cdot H_2O$, 2 g of NH_4Cl, 0.123 g of $N(CH_2CO_2Na)_3 \cdot H_2O$, 0.2 g of $MgSO_4 \cdot 7H_2O$, 0.012 g of $FeSO_4 \cdot 7H_2O$, 0.003 g of $MnSO_4 \cdot H_2O$, 0.003 g of $ZnSO_4 \cdot 7H_2O$, and 0.001 g of $CoCl_2 \cdot 6H_2O$ dissolved in 1000 mL of Milli-Q water and autoclaved at 121 °C. Cells were re-inoculated in BSM under the same conditions upon reaching visible light absorbance ($\lambda = 660$ nm) equal to 0.6 (Beckman DU 650, Fullerton, CA), which represents the midexponential phase of growth. The re-inoculation ensured subsequent rapid cell growth to stationary phase. The cells were harvested by centrifugation (10 000*g* for 10 min at 4 °C) upon reaching stationary phase (∼12 h)

* Corresponding author phone: (801) 581-5033; fax: (801) 581-7065; e-mail: wjohnson@mines.utah.edu.
[†] University of Utah.
[‡] Worcester Polytechnic Institute.

10.1021/es048850s CCC: $30.25
Published on Web 03/30/2005

with absorbance ($\lambda = 660$ nm) equal to about 1.2. Following centrifugation, the growth medium was decanted, and the pellet was resuspended in Narrow Channel artificial groundwater (NCAGW), a solution that reflects the groundwater from which DA001 was isolated (*17*). NCAGW consisted of 60 mg of $MgSO_4 \cdot 7H_2O$, 10 mg of KNO_3, 60 mg of $NaHCO_3$, 60 mg of $CaCl_2 \cdot 2H_2O$, 70 mg of $Ca(NO_3)_2 \cdot 4H_2O$, 25 mg of $CaSO_4 \cdot 2H_2O$, 0.4 mg of NaH_2PO_4 dissolved in 1000 mL of Milli-Q water. HCl (2 N) was used to adjust the pH to 6.0. The centrifugation−resuspension process was repeated three times to remove any trace of growth medium (BSM). Subsequently, the cells were starved at 15 °C for 48−72 h (shaking at 60 rpm) to stabilize their surface properties. Following starvation, cells were centrifuged and resuspended three times in NCAGW as described above. Cells were stained using 4′,6-diamidino-2-phenylindole (DAPI, Pierce, Rockford, IL) at a concentration in the cell suspension of 25 μg mL^{-1} with gentle vortexing for 20 min. Following staining, cells were centrifuged and resuspended three times in salt solution at the desired ionic strength (NaCl). Direct counts on an epifluoresence microscope were used to determine the stock concentration typically at the range of 10^8 to 10^9 cells mL^{-1}, which was diluted to obtain the target influent concentration of 1.5×10^4 ±50% cells mL^{-1}. The influent concentration of each experiment was 10^4 cells mL^{-1} to reflect relatively low concentrations of cells expected in groundwater. The influent concentration was normalized to 1.0×10^4 cells mL^{-1} to ease comparison between experiments.

The electrophoretic mobilities of starved and stained DA001 cells and crushed quartz sand were determined using a ζ analyzer (ZetaPALS, Brookhaven Instruments Corporation, Holtsville, NY) at a cell concentration of 10^7 cells mL^{-1}. Measurements were performed in NaCl solution with ionic strength ranging from 0.001 to 0.1 M at pH 6.72 and temperature equal to 8 °C to reflect experimental conditions. Electrophoretic mobilities were measured under different pH conditions at an ionic strength of 0.02 M. The pH adjustment was achieved by adding either 0.1 N HCl or 0.1 N NaOH to the cell suspensions, which yielded a maximum additional 10^{-5} M to the ionic strength. The electrophoretic mobility measurements were repeated 6−12 times. Measurements beyond an ionic strength of 0.1 M were not reproducible due to the low electrophoretic mobility, as well as due to heating of the highly conductive solution in the instrument.

Porous Media and Column Experiments. The porous media used for column experiments was 30−40 mesh (417−600 μm) quartz sand (Accusand, New Canaan, CT). The quartz sand was cleaned by soaking in concentrated HCl for at least 24 h, followed by repeated rinsing with Milli-Q water (Millipore Corp. Bedford, MA), drying at 105 °C, and baking overnight at 850 °C. The cleaned sand was stored under vacuum.

Prior to the column experiments, the cleaned quartz sand was rehydrated by boiling in Milli-Q water for at least 1 h. The cylindrical Plexiglass columns (20 cm in length and 3.81 cm in inner diameter) were dry-packed after the rehydrated quartz sand was dried at 105 °C and cooled. Packing was performed by adding quartz sand in small increments (∼2 cm) with mild vibration of the column with mild stirring between additions. A 60-mesh stainless steel screen (Gerard Daniel Worldwide, Hanover, PA) was placed at each end of the column. To spread the flow upon entry into the column, 3.5 g of coarse sand (>30 mesh, cleaned as described above) was added to the top of the influent screen, forming a 2 mm-thick layer that was covered by another screen.

The porosity of the packed quartz sand was determined gravimetrically to be 0.36. The mass of packed quartz sand in each column (∼390 g) differed by no more than 1%. The packed columns were purged with CO_2 for at least 25 min and then were preequilibrated with about 50 pore volumes of bacteria-free salt solution at pH 6.72, buffered by 0.005 M $NaHCO_3$. The additional ionic strength due to $NaHCO_3$ was on the order of 10^{-5} M. After preequilibration, the effluent pH was found to consistently differ by no more than 0.02 units from that of the influent. During initial preequilibration, a discontinuous air film was observed on the wall of the column. The air film was removed by the end of the first pore volume of preequilibration, as determined using a magnifying glass.

Following preequilibration, 3 pore volumes of suspended bacteria were injected into the column, followed by elution with 7 pore volumes of buffered salt solution (without bacteria) at the same ionic strength and pH. The suspensions and solutions were injected in up-flow mode using a syringe pump (Harvard Apparatus Inc., Holliston, MA). The pore volume based on tritiated water breakthrough agreed with the pore volume from weighing. This agreement, along with the symmetry of the tritiated water breakthrough, demonstrated uniform porosity within the column.

The transport experiments were carried out at three ionic strengths, 0.0038, 0.02, and 0.05 M. The flow rate was varied to produce pore water velocities of 2, 4, and 8 m day^{-1}. The experiments were run in a refrigerator (8 °C) to limit bacterial growth during the experiment. All the water used in the experiments had been autoclaved for sterility.

Samples from the column effluent were collected in sterile 5 mL polypropylene culture tubes (VWR, West Chester, PA) using a fraction collector (CF-1, Spectrum Chromatography, Houston, TX). The collected bacteria samples and reservoir samples were preserved using formaldehyde (1%) and were refrigerated at 4 °C until analysis (within several days). Following completion of the experiment, the sediment was extruded from the column and dissected into 10 segments (each 2 cm long). The attached bacteria were desorbed from the sediment segments into specific volumes of autoclaved Milli-Q water and were analyzed as described below.

The effluent and retained samples of DA001 were analyzed using ferrographic capture, a modified immunomagnetic technique. Ferrographic capture provides high-resolution analysis with a quantitation limit of 20 cells mL^{-1} (*15*, *18*). A standard DA001 suspension was analyzed for every 20 samples run to ensure accuracy. The standard deviation of replicate analyses of standards was less than 10%.

The number of bacteria that exited the column was determined by integration of the area under the breakthrough-elution curve. The cells recovered from all segments of the sediment were summed to determine the total number of retained cells. The overall recovery (mass balance) of cells was determined by summing the numbers of retained cells and cells that exited the column. The overall recovered number of cells was divided by the number of injected cells to express the mass balance as a percentage.

Atomic Force Microscopy Measurements and Modeling. The presence of extracellular polymers on DA001 was investigated using atomic force microscopy (AFM). The cells were grown in BSM and starved as described above, whereas in the case of the AFM measurements, the cells were resuspended into Milli-Q water (Milli-Q, Millipore Corp.) instead of NCAGW. Ideally, the solutions used in AFM and transport experiments would have been identical. Despite the differences in solution chemistry, the AFM experiments are sufficient to demonstrate the presence of extracellular polymers on DA001. Subsequent work will examine identical solution conditions to relate the deviations from log-linear retained profiles in quartz sand (observed here) and glass beads (*15*). Bacteria were attached to cleaned glass slides using an aminosilane compound, as described previously (*19*). Force measurements were performed and the data calibrated according to procedures described previously (*19*,

20), using silicon nitride cantilevers with spring constants of 0.13 N/m.

Each force cycle consists of an approach of the silicon nitride tip to the bacterium, and retraction of the tip after the two have been in contact. The approach data generally shows repulsion, and a model describing steric repulsion between the two surfaces was therefore applied. The steric force (F_{st}) as a function of the separation distance between the tip and sample (h) is given by

$$F_{st} = 50kTa_1L_o\Gamma^{3/2}\, e^{-2\pi h/L_o} \quad (1)$$

where k is the Boltzmann constant, T is the temperature, a_1 is the tip radius, Γ is the grafted polymer density in the brush layer reflecting the extent of surface coverage by polymers, h is the separation distance between the two surfaces, and L_o is the equilibrium height of the polymer brush layer.

Particle Tracking Model. The transport of DA001 was modeled using an advection−dispersion equation that includes removal from and re-entrainment to the aqueous phase:

$$\frac{\partial C}{\partial t} = -v\frac{\partial C}{\partial x} + D\frac{\partial^2 C}{\partial x^2} - k_f C + \frac{\rho_b}{\theta}k_r S_r \quad (2)$$

where C is the concentration of cells in the aqueous phase (cells per unit volume of fluid), t is the travel time, x is the travel distance, v is the flow velocity, D is the dispersion coefficient of the colloid particles, θ is the porosity, ρ_b is the bulk density of sediment, and k_f and k_r are rate coefficients for cell deposition to and re-entrainment from the solid phase, respectively. S_r is the reversibly retained bacterial concentration on the solid phase (cells per unit mass of sediment) and can be further expressed as

$$S_r = Sf_r \quad (3)$$

where S is the total deposited cell concentration and f_r is the fraction of reversibly retained cells.

A one-dimensional discrete random-walk particle-tracking model was used to solve eq 2 under the conditions of the column experiments, and details of implementation of the governing equation are given in other publications (*5*, *12*, *21*).

Filtration Theory. The deposition rate coefficients (k_f) can be calculated on the basis of filtration theory (eq 4 below), assuming a collision efficiency (α) equal to unity (absent a barrier to attachment).

$$k_f = \frac{3}{2}\frac{(1-\theta)}{d_c}\alpha\eta v \quad (4)$$

where θ is the sediment porosity, d_c is the collector (sediment grain) diameter, v is interstitial fluid velocity, and η is the collector efficiency. The value of the collector efficiency (η) can be determined using correlation equations available in the literature; that is, the R−T equation (*22*−*25*) and the T−E equation (*26*). Both correlation equations evaluate the collector efficiency based on regression of dimensionless parameters representing interception, sedimentation, and diffusion relative to numerical solution of convective-diffusion equation of particle transport in porous media.

Interaction Energy—Derjaguin, Landau, Verwey, and Overbeek (DLVO) Theory. DLVO theory was used to calculate the total interaction energy between bacterial cells and quartz sand as a function of separation distance. According to DLVO theory, the total interaction between two surfaces consists of van der Waals attraction, electrostatic interaction, and Born repulsion.

The geometry of interaction between a colloid and a much larger sand grain is reflected by that between a sphere and a plate. The electrostatic interaction energy between a sphere and a plate is given by Gregory (*27*) based on the linear superposition approximation.

$$\Delta G^{EL} = 64\pi\epsilon a_{colloid}\left(\frac{kT}{z_j e}\right)^2\gamma_1\gamma_2\exp(-\kappa h) \quad (5)$$

$$\gamma_i = \tanh\left(\frac{z_j e\psi_{0,i}}{4kT}\right) \quad (6)$$

$$\kappa = \sqrt{\frac{e^2\sum n_{j0}z_j^2}{\epsilon kT}} \quad (7)$$

where ϵ is the permittivity of the medium, z_j is the ion valence, e is the electron charge, $\psi_{0,i}$ is the surface potential (colloid or stationary phase surface), n_{j0} is the number concentration of ions in the bulk solution, $a_{colloid}$ is the colloid radius, and h is the separation distance. Surface potentials were approximated by ζ potentials calculated from the measured electrophoretic mobilities using the von Smoluchowski equation (*28*). The von Smoluchowski formula is based on a surface model in which the electric charges are located at the ideal ion-impenetrable surface of zero thickness.

The van der Waals attraction was calculated according to Gregory (*29*), who developed an expression that includes electromagnetic retardation.

$$\Delta G^{VDW} = -\frac{Aa_{colloid}}{6h}\left[1 - \frac{5.32h}{\lambda_o}\ln\left(1 + \frac{\lambda_o}{5.32h}\right)\right] \quad (8)$$

where A is the combined Hamaker constant for the bacteria−water−quartz sand system, 4.1×10^{-21} J (*30*), and λ_o is the "characteristic length" of the interaction, usually taken as 100 nm. The overlapping of electron orbits of two surfaces results in Born repulsion (*31*):

$$\Delta G^{Born} = \frac{A\sigma_c^6}{7560}\left[\frac{8a_{colloid}+h}{(2a_{colloid}+7)^7} + \frac{6a_{colloid}-h}{h^7}\right] \quad (9)$$

where the collision diameter, σ_c, was varied to achieve a primary minimum at the closest separation distance (d_o) at 0.158 nm (*32*).

Results

Electrokinetic Potentials. The influence of pH and ionic strength on the electrophoretic mobilities and ζ potentials of DA001 are presented in Figure 1 (top and bottom). At 0.02 M ionic strength, the ζ potential of DA001 was low, ranging from about +1.0 mV at pH 2 to about −1.5 mV at pH 6−10 (Figure 1, top). At pH 6.72 (the pH of the experiments), the ζ potential of DA001 was slightly negative (−1.6 mV) and became less negative with increasing ionic strength due to compression of the electrostatic double layer (Figure 1, bottom). The ζ potential of quartz sand decreased from about −70 to −50 mV over the ionic strength range from 0.0038 to 0.05 M (not shown).

Effluent Curves and Retained Profiles. Mass recoveries of bacteria from the transport experiments (total from effluent and sediment) were between 73% and 101% (Table 1) with the majority between 81% and 100%. The cells not recovered may represent inaccuracy in either effluent or sediment phase enumeration. However, the magnitude of the mass that was not accounted for is small relative to what is commonly observed in bacterial transport studies. The method of analysis, ferrographic capture, provides an unusually high resolution that supports examination of the relatively low

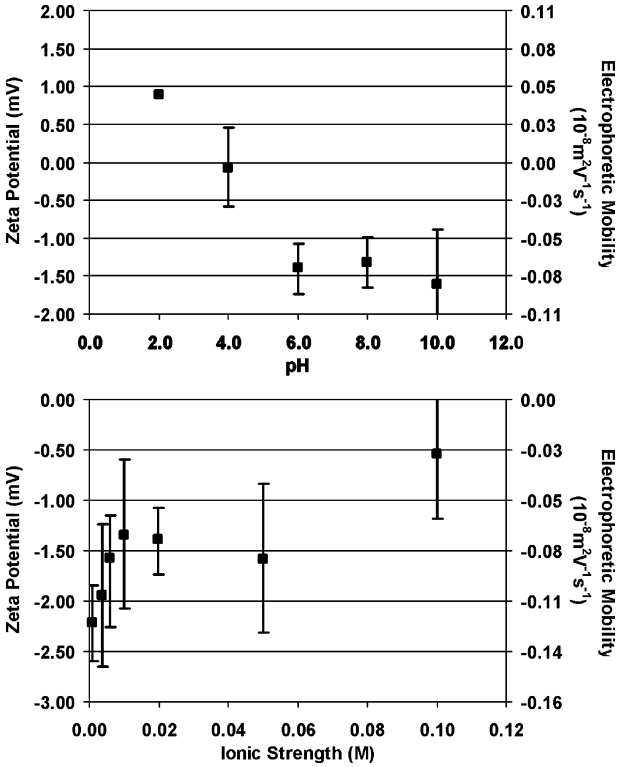

FIGURE 1. Effect of pH (top) and ionic strength (bottom) on electrophoretic mobilities and ζ potentials of DA001.

injection concentrations examined here. For the figures that follow (Figures 2−4), the relatively small mass that was unaccounted for was arbitrarily reapportioned equally (as percent) to the effluent and sediment by multiplying the cell numbers in those phases by an equivalent factor to close the mass balance.

The effluent breakthrough-elution curves and the retained profiles for bacteria at different ionic strengths are shown in Figure 2. Error bars in the effluent breakthrough-elution curves and the retained profiles represent standard deviations from replicate experiments ($n \geq 2$). The steady-state breakthrough plateaus were for the most part flat, indicating temporal constancy of the deposition rate coefficient (negligible blocking or ripening) during the course of the majority of the experiments. Steady-state breakthrough plateaus decreased negligibly with increased ionic strength (Figure 2 top) (8 m day^{-1}). The retained concentrations of DA001 insignificantly increased with increasing ionic strength (Figure 2, bottom), in correspondence with the effluent curves, as expected from mass balance considerations (Table 1).

The effluent breakthrough-elution curves and retained profiles of DA001 at different flow rates are shown for 0.05 M ionic strength (Figure 3) and 0.02 M ionic strength (Figure 4). The magnitude of the steady-state breakthrough plateaus varied insignificantly with increasing flow rate for both ionic strengths (Figure 3, top, and Figure 4, top). However, the profiles of retained DA001 provided detail that could not be observed in the breakthrough-elution curves; specifically, the concentrations of retained DA001 decreased and then increased with increasing flow rate for both ionic strengths (Figures 3 and 4, bottom).

Concentrations of retained bacteria decreased more rapidly than what was predicted based on a spatially constant first-order removal rate coefficient, as shown in Figures 2−4 (bottom). The simulations of the effluent breakthrough curves using a spatially constant deposition rate coefficient that honored the mass balance (dashed lines, Figures 2−4, top) were excellent; whereas the corresponding fits to the retained profiles (dashed lines, Figures 2−4, bottom) were poor, demonstrating the extent of hyperexponential deviation from log-linearity. The extent of deviation from log-linearity was unaffected by increased ionic strength or increased flow rate (Figures 2−4, bottom), as quantified by the standard deviation of the log-normal distribution of the deposition rate coefficient (σ ln k_f, Table 1), which did not decrease below a value of 4 despite the large increase in ionic strength. In contrast, σ ln k_f decreased from 5.3 to 1.8 over the ionic strength range 0.006 to 0.05 M for carboxylate-modified polystyrene latex microspheres (*12*).

Segments at or near the column outlet sometimes displayed increased retained concentrations relative to previous segments (typically at lower velocities), possibly reflecting longer DA001 residence time in the last segment and hence greater attachment. This could reflect stagnation of flow at the periphery of the packed column in the zone of convergence toward the outlet. This effect was not observed at the column inlet, possibly because flow was spread at the column inlet using a screened layer (2 mm) of larger sized grains.

Parallel experiments in quartz sand with different elution volumes (7 versus 14 pore volumes) showed no differences in the retained bacterial profiles (data not shown), indicating that detachment contributed insignificantly to the hyperexponential profiles observed in quartz sand. In contrast, the center of mass of the nonmonotonic retained profiles observed for DA001 in glass beads moved down-gradient in response to detachment (*15*).

Discussion

Hyperexponential decreases have been observed for many biological colloids (*1*−*4*, *8*, *10*). However, the results here contrast strongly against the nonmonotonic retained DA001 profiles that were obtained previously for DA001 in glass beads (*15*). That DA001 displayed hyperexponential deviations from log-linear behavior in quartz sand but nonmonotonic deviations in glass beads demonstrates that the form of deviation is sensitive to system conditions. Sensitivity of the form of deviation of retained profiles from log-linearity was recently shown for carboxylate-modified polystyrene microspheres (*12*, *16*). The cause of the nonmonotonic deviations is as yet unknown, whereas hyperexponential deviations have tentatively been attributed to distributions in surface properties among the colloid population (*12*).

Recently, soft particle electrophoresis theory was developed by Ohshima et al. (*28*, *33*) to determine surface potential from electrophoretic mobility in cases where charge distribution exists in an ion-penetrable surface layer of finite thickness. The theory has been applied to the electrophoretic mobility data of a number of microbial colloids, where the electrophoretic mobilities remain at nonzero values even at high ionic strengths (*34*, *35*). For DA001, the electrophoretic mobilities were slightly negative at low ionic strength and reached near-zero values at higher ionic strengths (Figure 1, bottom), suggesting that the von Smoluchowksi approach could be reasonably used to determine the ζ potentials given above.

The particle tracking model with log-normally distributed deposition rate coefficients (solid lines) simulated well the effluent curves (Figures 2−4, top). In contrast, this distributed k_f model could only approximate the shapes of the hyperexponential retained profiles (Figures 2−4, bottom), indicating that a log-normal distribution of k_f's among the bacterial population could not explain the observed retained profiles. Values for the deposition and re-entrainment rate coefficients (k_f and k_r) and the fraction of reversibly deposited cells (f_r) determined from simulations based on equal apportionment of missing mass between effluent and sediment are given in

TABLE 1. Experimental Conditions, Mass Balances, and Model Parameters for Simulations Using the Particle Tracking Model[a]

ionic strength (M)	pore water velocity (m-day^{-1})	recovery from effluent and sediment % total	recovery from sediment % total	distributed deposition rate coefficient				single deposition rate coefficient		
				mean k_f (h^{-1})	k_r (h^{-1})	SD n k_f	f_r	k_f (h^{-1})	k_r (h^{-1})	f_r
0.0038	8	89.42	2.9	1.84	2.8	5.50	0.90	0.15	1.20	0.65
0.02	8	81.31	7.7	3.17	1.0	6.55	0.55	0.16	0.65	0.16
0.05	8	76.50	4.1	2.86	1.57	6.70	0.65	0.155	0.90	0.24
0.02	2	101.00	6.1	3.56	3.0	4.50	0.98	0.11	0.35	0.77
0.02	4	73.00	2.6	1.29	2.0	4.20	0.90	0.09	0.80	0.60
0.05	2	100.00	5.6	3.10	3.0	4.50	0.98	0.08	0.35	0.70
0.05	4	74.00	2.4	0.76	0.5	4.50	0.80	0.068	0.40	0.60

[a] The parameter k_f is the deposition rate constant, the parameters f_r and k_r are the fraction of reversible deposition and the re-entrainment rate coefficient, respectively. The parameters ln k_f and σ ln k_f are the mean and standard deviation of the log-normal distribution of deposition rate coefficients, respectively.

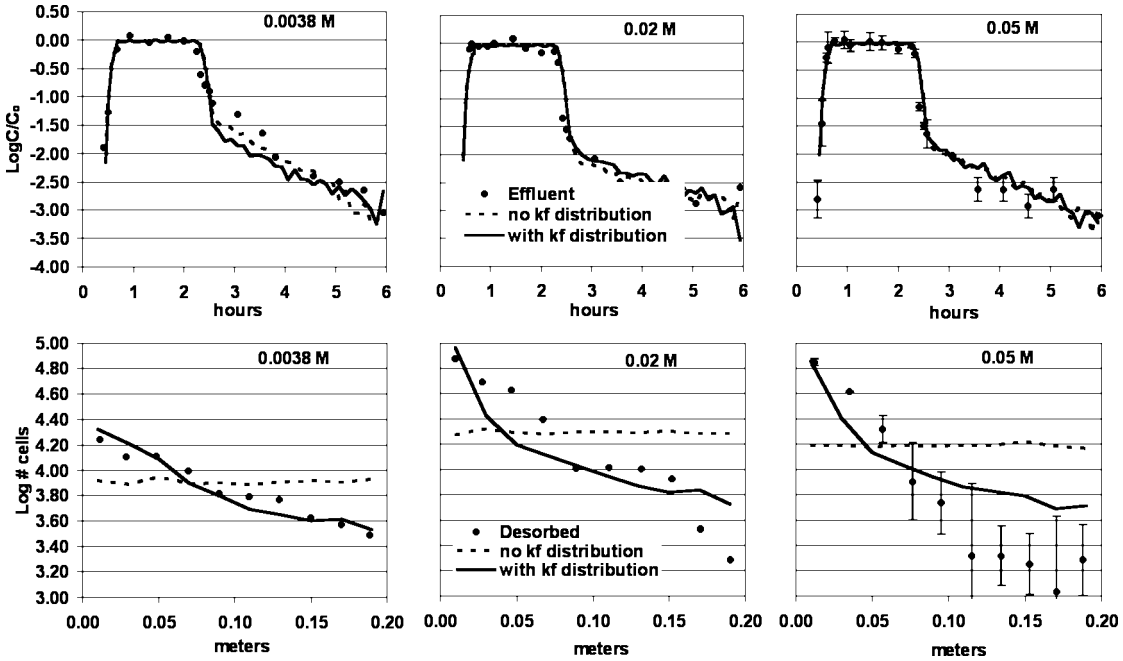

FIGURE 2. Ionic strength series for DA001 at flow rate = 8 m day^{-1}, showing effluent breakthrough-elution curves (top) and retained profiles (bottom). Error bars represent standard deviations in results from replicate experiments ($n \geq 2$). Simulations are shown from the particle tracking model using a single k_f (dashed line) and log-normally distributed k_f (solid line).

Table 1. The only clear trend that emerged from the model parameters was that reversibility of deposition (f_r) decreased with increasing flow rate, a result that is difficult to interpret given the complex surface and structural characteristics of bacteria.

In the absence of an energy barrier to attachment at 0.02 and 0.05 M ionic strength (Figure 5), all collisions between colloids and porous media grains are expected to be successful. Under these conditions, the collision efficiency (α) equals unity, and the magnitude of the deposition rate coefficient can be estimated using the correlation equations described above. Good agreement between measured and theory-based estimates of deposition rate in the absence of energy barriers has been demonstrated in this system using microspheres (*36*).

The magnitudes of the deposition rate coefficients (k_f) estimated using the T−E and R−T correlation equations (Figure 6) were orders of magnitude larger than those from the experiments (0.05 M condition shown as example) regardless of whether the unaccounted for mass was re-apportioned to the sediment (sediment-adjusted) or to the effluent (effluent-adjusted). Similar results were obtained for the 0.02 M condition (not shown) indicating that despite the absence of classic DLVO energy barriers at 0.02 and 0.05 M ionic strength (Figure 5), DA001 displayed low deposition. The adhesion deficiency of DA001 was apparently not controlled by electric double layer repulsion, but rather by non-DLVO processes, for example, hydration forces or steric interactions resulting from cell surface polymers. It should be noted that the values of k_f given in Table 1 are intermediate to those given in Figure 6, since the unaccounted for mass was re-apportioned equally between the sediment and effluent.

The extent of hyperexponential deviation of retained DA001 profiles in quartz sand from log-linear expectations did not decrease with increasing ionic strength (dashed line versus experimental data in Figure 2, bottom). In contrast, the carboxylate-modified polystyrene microspheres showed decreasing deviation from log-linear behavior with increasing ionic strength, and elimination of this deviation under favorable conditions (*12*, *16*). The carboxylate-modified microspheres showed strong negative ζ potentials that decreased with increasing ionic strength, indicating that in the case of the microspheres, deviation from log-linearity was driven by electrostatic repulsion. This contrast indicates that nonelectrostatic (non-DLVO) interactions are responsible for the ionic strength-independent deviations from log-linearity of the retained DA001 profiles.

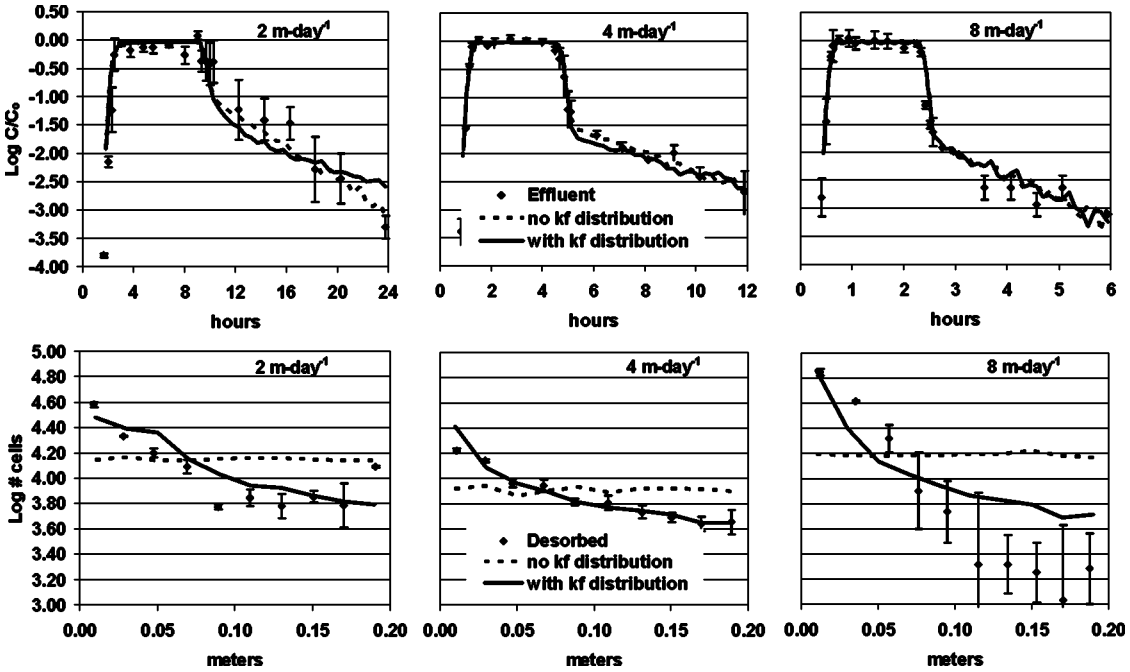

FIGURE 3. Flow rate series at ionic strength = 0.05 M for DA001, showing effluent breakthrough-elution curves (top) and retained profiles (bottom). Error bars represent standard deviations in results from replicate experiments ($n \geq 2$). Simulations are shown from the particle tracking model using a single k_f (dashed line) and log-normally distributed k_f (solid line).

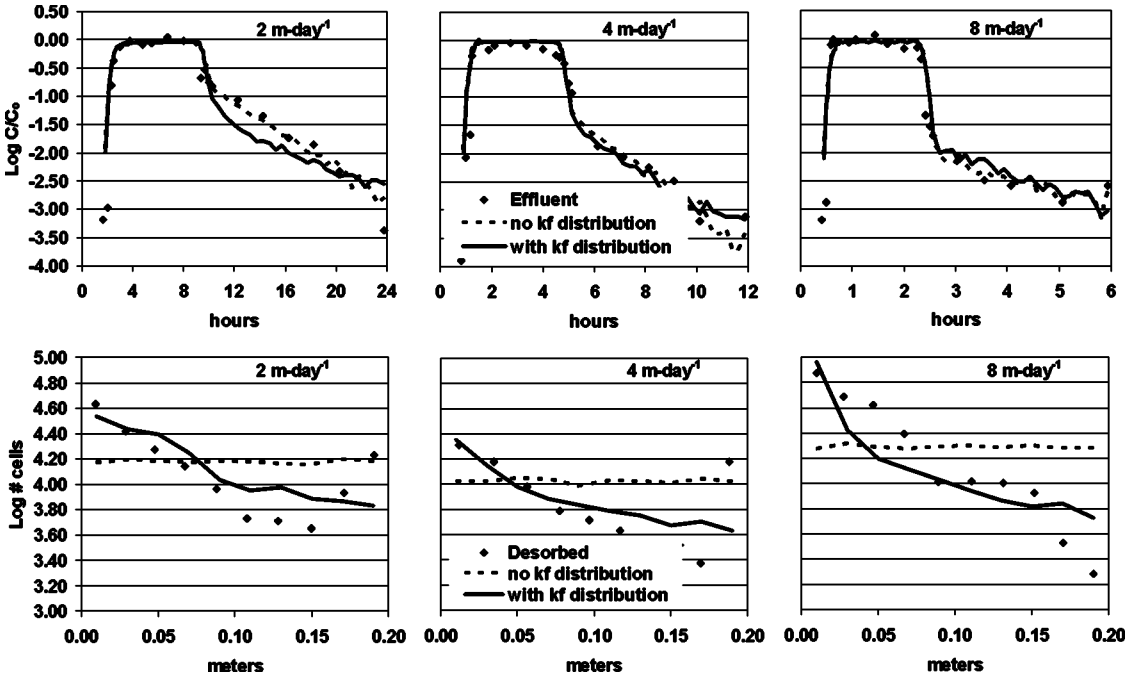

FIGURE 4. Flow rate series at ionic strength = 0.02 M for DA001, showing effluent breakthrough-elution curves (top), and retained profiles (bottom). Simulations are shown from the particle tracking model using a single k_f (dashed line) and log-normally distributed k_f (solid line).

AFM experiments revealed that the surface of DA001 possesses polymers that range from tens to hundreds of nanometers. When the steric model was applied to AFM approach curves (Figure 7, top), polymers were calculated to extend on average 59.8 nm from the cell surface. The polymer extensions were distributed from 12.2 to 104.7 nm (Figure 7, bottom). These extensions provide for steric repulsive forces that are much larger than DLVO-type interactions (*37*) and that occur over much larger separation distances than DLVO interactions (Figure 5).

In addition, the affinity of the surface polymers to silicon nitride was rather low compared with other bacteria we have studied, such as *Pseudomonas putida* KT2442 (*19*) and *Eschericia coli* JM109 (*38*). The retraction curves for DA001 were characterized by many weak adhesion events (Figure 8, top). Although 14 force cycles were captured, 51 adhesion events were observed that ranged from −0.03 to −1.0 nN (Figure 8, bottom). Hence, each time the AFM tip approached the bacterium, the tip contacted multiple polymers. These results suggest the presence of a dense polymer brush on the surface of DA001.

Silicon nitride has been found to be a reasonable model for quartz sand, since both are smooth surfaces and have similar ζ potentials at neutral pH (*38*−*40*). The low affinity

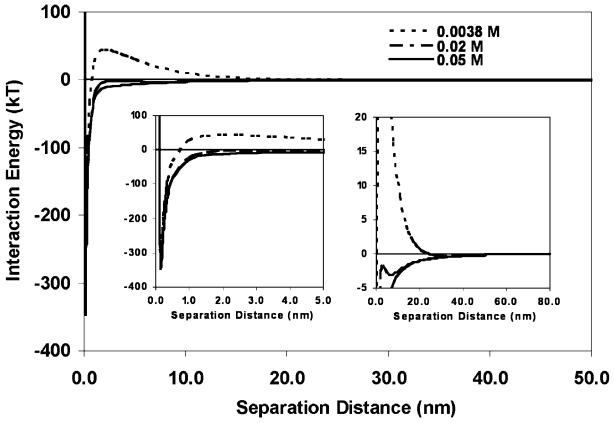

FIGURE 5. DLVO interaction energy profiles at different ionic strengths (pH = 6.72). Insets highlight the locations of the primary energy minima (left) and the secondary energy minima (right).

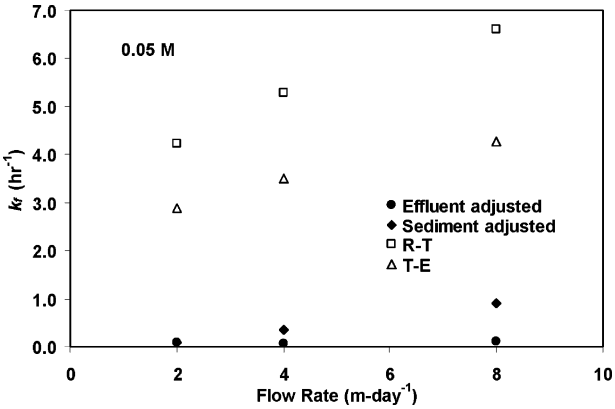

FIGURE 6. Experimental and filtration theory-based deposition rate coefficients (k_f) versus flow rate at 0.05 M ionic strength. The term "effluent-adjusted" refers to re-apportioning all unaccounted for mass to effluent, whereas the term "sediment-adjusted" refers to re-apportioning all unaccounted for mass to the sediment. The mass transport-supported deposition rate coefficients were estimated using the R−T and T−E equations.

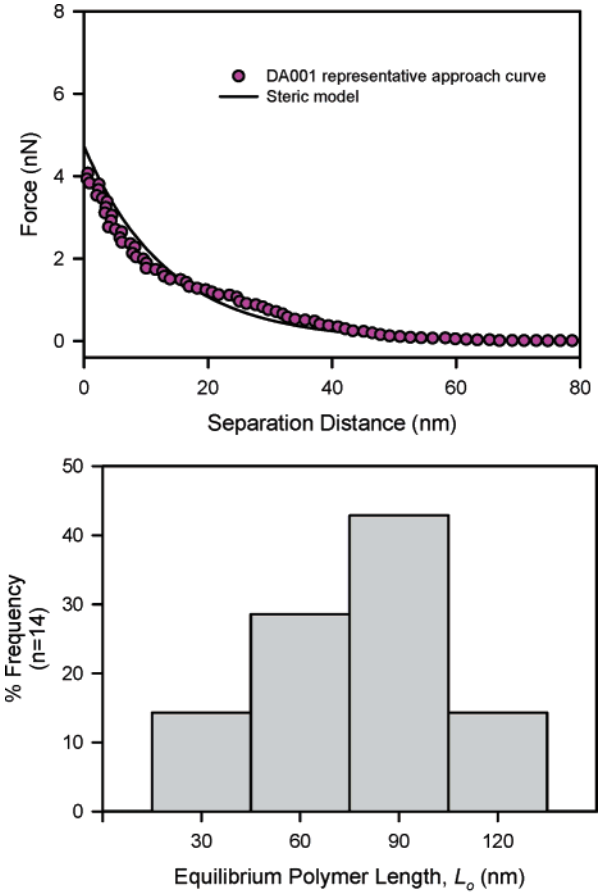

FIGURE 7. Representative approach curve and steric model results for DA001 in water. Fourteen approach curves were captured on three bacterial cells. An example (top) is shown of the approach curve with the steric model result (L_o = 84.6 nm, $\Gamma = 1.06 \times 10^{16}$ m^{-2}, and $R^2 = 0.96$). The distribution of equilibrium polymer lengths on DA001 in water is also shown (bottom). The average polymer length is 59.8 nm. Polymer lengths were obtained by fitting the approach curves with the steric model (eq 1).

of DA001 surface polymers for silicon nitride is consistent with the low adhesion to quartz observed in the column experiments.

Extracellular polymers have been well demonstrated to govern the adhesion of bacteria to surfaces (*37*, *38*, *40*−*44*). Camesano et al. (*37*) found a substantial reduction in the magnitude and decay length of the repulsive forces in response to partial removal of extracellular polysaccharides from strains KT2442 and G4. Jucker et al. (*41*, *42*) showed that differences in lipopolysaccharide (LPS) lengths enhanced adhesion, whereas the existence of a dense brush of LPS on similar lengths resulted in low adhesion. For example, bacterial strain DSM 50170, with 99.5% short LPS (1 nm) and 0.5% long LPS (30 nm), showed greater adhesion to glass than four other bacterial strains that carried only long LPS. Dong et al. (*44*) found via polyacrylamide gel electrophoresis that bacterial strain DA001 produced LPS. The AFM results reported here are consistent with the possibility that a dense extracellular polymer brush governs the adhesion deficiency of DA001.

The possibility that extracellular polymers govern the low adhesion and deviation from log-linear retained profiles for DA001 is also indicated by previous experiments performed in glass bead porous media (*15*). In the glass bead system, the pH of the solution was allowed to increase from 6.0 to 9.4 across the length of the column (absence of buffer). Increases in ionic strength in the glass bead system yielded large increases in the bacterial deposition rate constant, a result that was not observed here in the quartz porous media. In the absence of other considerations, the observed increase in deposition rate with increased ionic strength in the glass bead system would be considered consistent with classic DLVO considerations, that is, compression of the electrostatic double layer with increased ionic strength. However, the retained bacterial profiles in the glass beads revealed that deposition increases were accompanied by a change from hyperexponential to nonmonotonic deviations from log-linearity, a result that cannot be explained by mere compression of the electric double layer or by increased pH along the length of the column, which would (according to classic DLVO theory) increase repulsion between the overall negatively charged surfaces. Furthermore, the reversibility of deposition (f_r) increased greatly with increasing ionic strength in the glass bead system, another result that is not explained by classic DLVO considerations. The drastic change in the form of the retained profiles and the large increase in the reversibility of deposition require explanation by more complex mechanisms than those represented in classic DLVO theory. These changes suggest the presence of cell surface polymers that change conformation with pH and ionic strength.

This work has demonstrated that retained profiles of bacterial strain DA001 in quartz sand were hyperexponential in form, contrasting strongly against the nonmonotonic profiles obtained for carboxylate-modified microspheres in

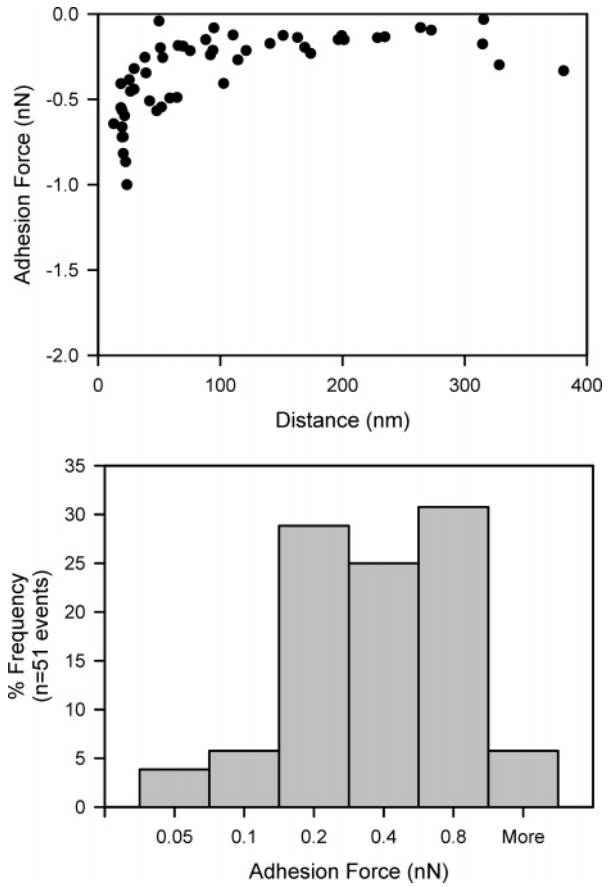

FIGURE 8. Distribution of adhesion forces between DA001 and silicon nitride in water. The maximum adhesion force for each pull-off event is shown (top) with the distance at which pull-off occurs. The histogram of the distribution of pull-off events between DA001 and silicon nitride in water is also shown (bottom). Fourteen force cycles were captured on three bacterial cells. All of the force cycles had multiple adhesion events, resulting in a total of 51 adhesion events. Each instance where a polymer from DA001 attaches to the AFM tip and detaches is defined as a discrete adhesion event.

the same porous media under the same conditions. This result also contrasts against the nonmonotonic retained DA001 profiles obtained in glass bead porous media. These two contrasts demonstrate that the form of deviation from log-linear expectations is sensitive to system conditions. The deposition rate coefficients for DA001 in quartz sand were orders of magnitude below expectations from filtration theory despite the absence of a classic DLVO energy barrier. This and above-described aspects of the retained bacterial profiles in quartz sand and glass bead porous media suggest the influence of non-DLVO mechanisms in DA001 adhesion deficiency, specifically steric interactions associated with cell surface polymers. Adhesion force measurements made using AFM in pure water demonstrated the presence of cell surface polymers on DA001, which averaged 59.8 nm in their extension from the cell surface, indicating prevalence of steric interactions from polymers with low affinity for the model surface, silicon nitride. The low affinities of the polymers for silicon nitride suggest low affinities for quartz sand, consistent with the low adhesion observed in the transport experiments.

Acknowledgments

This work was funded by a grant from the National Science Foundation Hydrologic Sciences Program (Grant EAR 0087522) to W.P. Johnson. Any opinions, findings, and conclusions or recommendations expressed in this material are those of the authors and do not necessarily reflect the views of the National Science Foundation. Shambralynn Baker and Theresa Diester assisted with the porous media transport experiments. Justin R. Johnson, Jeffrey Pouliot, and Jeffrey Savard assisted with the AFM experiments.

Literature Cited

(1) Albinger, O.; Biesemeyer, B. K.; Arnold, R. G.; Logan, B. E. Effect of bacterial heterogeneity on adhesion to uniform collectors by monoclonal populations. *FEMS Microbiol. Lett.* **1994**, *124* (3), 321−326.

(2) Baygents, J. C.; Glynn, J. R., Jr.; Albinger, O.; Biesemeyer, B. K.; Ogden, K. L.; Arnold, R. G. Variation of surface charge density in monoclonal bacterial populations: implications for transport through porous media. *Environ. Sci. Technol.* **1998**, *32* (11), 1596−1603.

(3) Simoni, S. F.; Harms, H.; Bosma, T. N. P.; Zehnder, A. J. B. Population heterogeneity affects transport of bacteria through sand columns at low flow rates. *Environ. Sci. Technol.* **1998**, *32* (14), 2100−2105.

(4) Bolster, C. H.; Mills, A. L.; Hornberger, G.; Herman, J. Effect of intra-population variability on the long-distance transport of bacteria. *Ground Water* **2000**, *38* (3), 370−375.

(5) Zhang, P.; Johnson, W. P.; Scheibe, T. D.; Choi, K.; Dobbs, F. C.; Mailloux, B. J. Extended tailing of bacteria following breakthrough at the Narrow Channel Focus Area, Oyster, Virginia. *Water Resour. Res.* **2001**, *37* (11), 2687−2698.

(6) Deflaun, M. F.; Murray, C. J.; Holben, M.; Scheibe, T.; Mills, A.; Ginn, T.; Griffin, T.; Majer, E.; Wilson, J. L. Preliminary observations on bacterial transport in a coastal plain aquifer. *FEMS Microbiol. Rev.* **1997**, *20* (3−4), 473−487.

(7) Harvey, R. W.; Garabedian, S. P. Use of colloid filtration theory in modeling movement of bacteria through a contaminated sandy aquifer. *Environ. Sci. Technol.* **1991**, *25* (1), 178−185.

(8) Harter, T.; Wagner, S.; Atwill, E. R. Colloid transport and filtration of cryptosporidium parvum in sandy soils and aquifer sediments. *Environ. Sci. Technol.* **2000**, *34* (1), 62−70.

(9) Gerba, C. P.; Lance, J. C. Poliovirus removal from primary and secondary sewage effluent by soil filtration. *Appl. Environ. Microbiol.* **1978**, *36* (2), 247−251.

(10) Redman, J. A.; Grant, S. B.; Olson, T. M.; Estes, M. K. Pathogen filtration, heterogeneity, and the potable reuse of wastewater. *Environ. Sci. Technol.* **2001**, *35* (9), 1798−1805.

(11) Bales, R. C.; Li, S. M.; Yeh, T. C. J.; Lenczewski, M. E.; Gerba, C. P. Bacteriophage and microsphere transport in saturated porous media: forced-gradient experiment at Borden, Ontario. *Water Resour. Res.* **1997**, *33* (4), 639−648.

(12) Li, X.; Scheibe, T. D.; Johnson, W. P. Apparent decreases in colloid deposition rate coefficient with distance of transport under unfavorable deposition conditions: a general phenomenon. *Environ. Sci. Technol.* **2004**, *38* (21), 5616−5625.

(13) Tufenkji, N.; Elimelech, M. Deviation from classical colloid filtration theory in the presence of repulsive DLVO interactions. *Langmuir*. **2004**, *20* (25), 10818−10828.

(14) Bradford, S. A.; Yates, S. R.; Bettahar, M.; Simunek, J. Physical factors affecting the transport and fate of colloids in saturated porous media. *Water Resour. Res.* **2002**, *38* (12), 1327−1338.

(15) Tong, M.; Li, X.; Brow, C.; Johnson, W. P. Detachment-influenced transport of an adhesion-deficient bacterial strain within water-reactive porous media. *Environ. Sci. Technol.* **2005**, *39*(8), 2500−2508.

(16) Li, X.; Johnson, W. P. Nonmonotonic variations in deposition rate coefficients of microspheres in porous media under unfavorable deposition conditions. *Environ. Sci. Technol.* **2005**, *39*(6), 1658−1665.

(17) DeFlaun, M. F.; Fuller, M. E.; Zhang, P.; Johnson, W. P.; Mailloux, B. J.; Holben, W.; Kovacik, W.; Balkwill, D.; Onstott, T. C. Comparison of methods for monitoring bacterial transport in the subsurface. *J. Microbiol. Methods* **2001**, *47* (2), 219−231.

(18) Zhang, P.; Johnson, W. P.; Rowland, R. Bacteria tracking using ferrographic separation. *Environ. Sci. Technol.* **1999**, *33* (14), 2456−2460.

(19) Abu-Lail, N. I.; Camesano, T. A. Role of ionic strength on the relationship of biopolymer conformation, DLVO contributions, and steric interactions to bioadhesion of *Pseudomonas putida* KT2442. *Biomacromolecules.* **2003**, *4* (4), 1000−1012.

(20) Emerson, R. J. IV.; Camesano T. A. A nanoscale investigation of pathogenic microbial adhesion in biomaterial systems. *Appl. Environ. Microbiol.* **2004**, *70* (10), 6012−6022.

(21) Scheibe, T. D.; Wood, B. D. A particle-based model of size or anion exclusion with application to microbial transport in porous media. *Water Resour. Res.* **2003**, *39* (4), doi: 10.1029/2001WR001223.

(22) Rajagopalan, R.; Tien, C. Trajectory analysis of deep-bed filtration with the sphere-in-cell porous media mode. *AIChE J.* **1976**, *22* (3), 523−533.
(23) Rajagopalan, R.; Tien, C.; Pfeffer, R.; Tardos, G. Letter to the editor. *AIChE J.* **1982**, *28* (5), 871−872.
(24) Tien, C. Mass. *Granular filtration of aerosols and hydrosols*; Butterworths Series in Chemical Engineering; Butterworths: Boston, MA, 1989; Vol. 1.
(25) Logan, B. E.; Jewett, D. G.; Arnold, R. G.; Bouwer, E. J.; O'Melia, C. R. Clarification of clean-bed filtration models. *J. Environ. Eng.* **1995**, *121* (12), 869−873.
(26) Tufenkji, N.; Elimelech, M. Correlation equation for predicting single-collector efficiency in physicochemical filtration in saturated porous media. *Environ. Sci. Technol.* **2004**, *38* (2), 529−536.
(27) Gregory, J. Interaction of unequal double layers at constant change. *J. Colloid Interface Sci.* **1975**, *51* (1), 44−51.
(28) Ohshima, H. Electrophoretic mobility of soft particles. *Colloids Surf., A* **1995**, *103* (3), 249−255.
(29) Gregory, J. Approximate expressions for retarded van der Waals interaction. *J. Colloid Interface Sci.* **1981**, *83* (1), 138−145.
(30) Dong, H.; Onstott, T. C.; Ko, C. H.; Hollingsworth, A. D.; Brown, D. G.; Mailloux, B. J. Theoretical Prediction of Collision Efficiency Between an Adhesion-Deficient Bacterium and Aquifer Sediments. *Colloids Surf., B* **2002**, *24* (3−4), 229−245.
(31) Ruckenstein, E.; Prieve, D. C. Adsorption and desorption of particles and their chromatographic separation. *AIChE J.* **1976**, *22* (1), 276−285.
(32) Van Oss, C. J. *Interfacial Forces in Aqueous Media*; Marcel Dekker: New York, 1994.
(33) Ohshima, H. Electrophoretic mobility of soft particles. *J. Colloids Interface Sci.* **1994**, *163* (2), 474−483.
(34) Morisaki, H.; Nagai, S.; Ohshima, H.; Ikemoto, E.; Kogue, K. The effect of mobility ad cell-surface polymer on bacterial attachment. *Microbiology* **1999**, *145* (10), 2797−2802.
(35) Hayashi, H.; Tsuneda, S.; Hirata, A.; Sasaki, H. Soft particle analysis of bacterial cells and its interpretation of cell adhesion behaviors in terms of DLVO theory. *Colloids Surf., B* **2001**, *22* (2), 149−157.
(36) Li, X.; Zhang, P.; Lin, C. L.; Johnson, W. P. Effect of Hydrodynamic Drag on Microsphere Deposition and Re-entrainment under Unfavorable Conditions. *Environ. Sci. Technol.*, **2005**, in press.
(37) Camesano, T. A.; Logan. B. E. Probing bacterial electrosteric interactions using atomic force microscopy. *Environ. Sci. Technol.* **2000**, *34* (16), 3354−3362.
(38) Abu-Lail, N. I.; Camesano, T. A. Role of lipopolysaccharides in the adhesion, retention, and transport of *Escherichia coli* JM109. *Environ. Sci. Technol.* **2003**, *37* (10), 2173-2183.
(39) Johnson, P. R. A comparison of streaming and microelectrophoresis methods for obtaining the ζ potential of granular porous media surfaces. *J. Colloid Interface Sci.* **1999**, *209* (1), 264−267.
(40) Zhmud, B. V.; Sonnefeld, J.; Bergstrom, L. Influence of chemical pretreatment on the surface properties of silicon nitride powder. *Colloids Surf., A* **1999**, *158* (3), 327−341.
(41) Jucker, B. A.; Harms, H.; Zehnder, A. J. B. Polymer interactions between five gram-negative bacteria and glass investigated using LPS micelles and vesicles as model systems. *Colloids Surf., B* **1998**, *11* (1−2), 33−45.
(42) Jucker, B. A.; Zehnder, A. J. B.; Harms, H. Quantification of polymer interactions in bacteria adhesion. *Environ. Sci. Technol.* **1998**, *32* (19), 2909−2915.
(43) DeFlaun, M. F.; Oppenheimer, S. R.; Condee, C. W.; Fletcher, M. Alterations in adhesion, transport, and membrane characteristics in an adhesion-deficient pseudomonad. *Appl. Environ. Microbiol.* **1999**, *65* (2), 759−765.
(44) Dong, H.; Rothmel, R.; Onstott, T. C.; Fuller, M. E.; DeFlaun, M. F.; Streger, S. H.; Dunlap, R.; Fletcher, M. Simultaneous transport of two bacterial strains in Intact cores from Oyster, Virginia: biological effects and numerical modeling. *Appl. Environ. Microbiol.* **2002**, *68* (5), 2120−2132.

Received for review July 23, 2004. Revised manuscript received February 24, 2005. Accepted March 1, 2005.

ES048850S